POLITECNICO DI TORINO
Repository ISTITUZIONALE

Internal forces measured in segmental tunnel linings compared with numerical predictions obtained from state-of-the-art calculation methods used in engineering practice

Original
Internal forces measured in segmental tunnel linings compared with numerical predictions obtained from state-of-the-art calculation methods used in engineering practice / Rauch, F., Oreste, P., Fischer, O.. - In: TUNNELLING AND UNDERGROUND SPACE TECHNOLOGY. - ISSN 0886-7798. - STAMPA. - 154:(2024), pp. 1-14. [10.1016/j.tust.2024.106084]

Availability:
This version is available at: 11583/2996341 since: 2025-01-07T15:21:04Z

Publisher:
Elsevier Ltd.

Published
DOI:10.1016/j.tust.2024.106084

Terms of use:

This article is made available under terms and conditions as specified in the corresponding bibliographic description in the repository

Publisher copyright
Elsevier postprint/Author's Accepted Manuscript

© 2024. This manuscript version is made available under the CC-BY-NC-ND 4.0 license http://creativecommons.org/licenses/by-nc-nd/4.0/.The final authenticated version is available online at: http://dx.doi.org/10.1016/j.tust.2024.106084

(Article begins on next page)

10 October 2026

Tunnelling and Underground Space Technology 154 (2024) 106084

Contents lists available at ScienceDirect

Tunnelling and Underground Space Technology incorporating Trenchless Technology Research

journal homepage: www.elsevier.com/locate/tust

Internal forces measured in segmental tunnel linings compared with numerical predictions obtained from state-of-the-art calculation methods used in engineering practice

Fabian Rauch [a], Pierpaolo Oreste [b,*], Oliver Fischer [a]

[a] Chair of Concrete and Masonry Structures, School of Engineering and Design, Technical University of Munich, Theresienstraße 90, 80333 Munich, Germany
[b] Department of Environment, Land and Infrastructure Engineering (DIATI), Politecnico di Torino, Corso Duca degli Abruzzi 24, 10129 Torino, Italy

ARTICLE INFO

Keywords:
TBM
Structural design
FEM
Structural monitoring
In-situ measurements
Simulation

ABSTRACT

Different calculation methods and modeling strategies are commonly used in engineering practice to predict the internal forces in segmental tunnel linings. Accordingly, the calculation results can differ. The present paper compares internal forces resulting from five state-of-the-art calculation models, of which three continuum models and two bedded beam models, to new in-situ measurements of internal forces at the recently built TBM tunnel for the U5 metro line in Frankfurt, Germany, and discusses agreements and differences. Hereby, a generally good agreement is found for the normal forces. The predictions of the bending moments are satisfying, but there are some discrepancies. It is shown that it might be necessary to consider assembly imperfections in the calculation models to improve the agreement between the calculation results and the measurements. Also, the differences between the calculation methods themselves are addressed. It is analyzed that generally continuum models give more realistic internal forces, but that also bedded beam models can have advantages, e.g. when large parametric studies are required. Finally, recommendations are given regarding the application of calculation models for structural design.

1. Introduction

In TBM tunneling, a segmental tunnel lining is formed by assembling reinforced or steel fiber concrete segments into rings. The structural design of the segments needs to ensure their stability, serviceability, and durability. This requires predicting the internal forces and the stresses related to them in the lining accurately (enough). However, these predictions are challenging engineering tasks due to several reasons. On the one hand, the nature of the segmented structure requires that several complex interactions occur between the components involved: between the single segments ("longitudinal joints"), between neighboring rings ("ring or circumferential joints"), and between lining and soil ("soil-lining interface"). It can be challenging to determine realistic characteristics for interactions and interfaces to model and simulate these interactions and their effects accurately. Consequentially, this adversely affects the accuracy of calculation results. On the other hand, incomplete knowledge of parameters, e.g., of the surrounding soil – which causes the main loading – and time-dependent mechanisms, contribute to the uncertainties and inaccuracies regarding the predicted stresses and internal forces in segmental linings.

Nevertheless, shield-driven tunneling has experienced significant technical progress over the last few decades, especially regarding mechanical engineering (Fischer et al., 2014). Tunnels can now be realized very variably under almost all geological and hydrological situations and the most complex boundary conditions (Thewes, 2014), e.g. in densely populated urban areas with low overburden (Schade et al., 2023) or with high diameters (Grübl, 2012), and this development allows them to contribute more to a sustainable and efficient infrastructure (Bobylev et al., 2023; Sauer, 2016).

Because the boundary conditions can be quite complex, reliable and accurate predictions regarding the structural behavior of segmental linings are necessary. This includes stresses and internal forces in the linings, which are addressed in this paper, but also the influence of shield-driven tunneling on other structures e.g. in settlement predictions. Inaccurate or erroneous calculations can lead to interruptions of construction works, delays in construction progress, increased costs, damage and subsequent refurbishments, reduced durability, and in extreme cases to danger for people.

* Corresponding author.
E-mail address: pierpaolo.oreste@polito.it (P. Oreste).

https://doi.org/10.1016/j.tust.2024.106084
Received 24 February 2024; Received in revised form 5 June 2024; Accepted 11 September 2024
Available online 26 September 2024
0886-7798/© 2024 The Authors. Published by Elsevier Ltd. This is an open access article under the CC BY license (http://creativecommons.org/licenses/by/4.0/).

Significant technical developments regarding the calculation methods for segmental tunnel linings have also occurred over the last few decades to ensure flawless tunnel linings (Fischer et al., 2014; Meschke, 2014). Modern calculation methods can accurately consider many aspects and mechanisms of shield-driven tunneling and segmented linings. Their level of detail can reach up to the time-dependent three-dimensional simulation of the complete construction procedure (Marwan, 2019; Marwan et al., 2021; Meschke et al., 2023) and consider highly complex situations (Zaheri and Ranjbarnia, 2021; Zaheri and Ranjbarnia, 2022; Zaheri et al., 2022), which, however, is not always suited for common practical applications.

However, although modern calculation methods are widely used in engineering practice, their results have rarely been compared to in-situ measurements due to limited available measurement data. In a recent long-term monitoring campaign that is presented in section 3 and was carried out by two of the authors, new measurement data regarding the internal forces in a segmental tunnel lining was gained and validated by complementary laboratory tests. This paper compares the results of different calculation models that align with the state-of-the-art to these measurement data. The study concerns the long-term, final state internal forces, the normal forces and the bending moments.

2. Calculation methods

Nowadays, in engineering practice, two general types of calculation methods are common and widely used for the structural design of the lining itself: “continuum models” and “bedded beam (or also frame) models”. Further analytical and strongly simplified methods are sometimes suited for validations and to get quick results. Due to their high degree of simplification, they are not part of this paper.

In continuum models (e.g. Do and Dias, 2017; Möller, 2006; Kolymbas, 2008), the lining and the soil are modeled explicitly. Gravity causes loads that act on the lining (“passive loading”). With continuum models it is possible to simulate the development of stresses in and deformations of the soil and the lining. The lining itself can be modeled with a one-dimensional (1D) beam chain (e.g. Do, 2014) or with its real geometry (e.g. Marwan, 2019). In 1D lining models, the behavior of longitudinal joints can be considered with rotational springs according to Janßen (1983), who adopted the concrete hinge relationship of Leonhardt and Reimann (1966) for segmental linings; in higher dimensionalities, interface elements or contact formulations can be applied (Marwan, 2019), or they can generally be neglected if other aspects are of interest (e.g. Smarslik et al., 2017). The interaction between the lining and the soil is either modeled explicitly with interface elements or contact formulations, or is considered rigid.

In contrast, numerical bedded beam models (e.g. Behnen et al., 2013, 2015; Fischer et al., 2014; Oreste, 2007), commonly represent the lining with a chain of one- (1D) or two-dimensional (2D) beams. In these models, the “soil” – or, more accurately, the soil-lining interaction – is modeled with independent springs (Duddeck, 1980). Consequently, the loads acting on the lining must be applied directly (“active loading”). The effect of the longitudinal joint can be modeled similarly to continuum models.

Various state-of-the-art, international recommendations and guidelines (ACI, 2020; BMVI, 2022; DAUB, 2014, 2024; DB-Netze, 2014; DGGT, 2014a; ITA, 2019; ÖVBB, 2009) generally do allow the utilization of both methods in structural design and both have been used successfully. Some of them recommend the usage of continuum models in soft soil or in the case of complex geometries or loadings (ACI, 2020; DAUB, 2024; ÖVBB, 2009). Further various, justifiable modeling approaches and strategies are possible within the two methods.

Both calculation methods can be applied for two (2D) – and three-dimensional (3D) simulations. In 3D simulations, also the longitudinal interactions of neighboring rings can be considered. In most cases, a 2D model with plane strain conditions is sufficient (Bakhshi and Nasri, 2014a, 2014b; DAUB, 2024; DGGT, 2014b; ITA, 2019) and, if relevant, 3D effects as ground relaxations following excavation can be considered with suitable deconfinement methods (Meschke, 2014). 3D models are, however, required if spatial mechanisms, concentrated loads, or local geometry changes, as in cross-passage areas, occur and influence the tunnel lining (DAUB, 2024; Klappers et al., 2006; ÖVBB, 2009). Also, if the early stages are of interest and the construction procedure is simulated explicitly, 3D models are required (ACI, 2020; Bakhshi and Nasri, 2014b; DAUB, 2024; ÖVBB 2009). Despite the developments in computer technology, full 3D models still nowadays require an elevated calculation time and are, therefore, not always suited for engineering practice, particularly for large parametric studies (DAUB, 2024). This is why, although the structural behavior of a tunnel is three-dimensional (Arnau and Molins, 2012), 2D and “quasi/pseudo-3D” calculations are widely used (Do and Dias, 2017) and are also the main concern of this paper.

3. The studied case

In Frankfurt (Main), Germany, the U5 metro line was extended by an 840 m long shield-driven tunnel to connect a newly built city district to the city’s public transport network (Budach et al., 2020). In the eastern part, the tunnel route (Fig. 1) crosses an area with several existing and planned skyscrapers that are about to be constructed in the upcoming years. In particular, a 175 m tall skyscraper will be built on the route and will eventually be positioned right above the tunnel. In this area, with a ratio of overburden to diameter of about 1.95, the U5 can be considered a shallow tunnel. It will be strongly affected by the skyscraper construction and the corresponding excavation pits. This was also observed in preceding calculations (ARGE SBEV, 2017). Therefore, to survey the structural behavior of the tunnel before, during, and after the skyscraper construction, a structural monitoring campaign was applied to the lining by two of the authors, during which the measurement data for the analyses in this paper was gained. The monitoring campaign and the relevant results are summarized subsequently. More details can be found in Rauch and Fischer (2022, 2023, 2024a).

The lining of the U5 consists of six reinforced concrete segments of equal size placed in a staggered configuration with a 30-degree offset between subsequent rings. The segments are named clockwise with letters from A to E and keystone K (Fig. 1). The lining has an inner diameter of 5.90 m, a thickness of 45 cm, and a single ring length of 1.20 m. The longitudinal joints are of plane shape. Their contact surface has a width of 25 cm, and its center line is aligned with the segment’s center line. The ring joints are also plane. The contact between two rings occurs through twelve plywood packers. Two of them are placed on each segment’s side and positioned in line with the tunnel boring machine’s (TBM) jacks. Bolts are used as assembly aids but are removed after some days and are not part of the final state lining. The segment’s concrete is a C45, with a Young’s modulus of about 36000 N/mm2. The bending reinforcement consists of 13 B500 steel bars with a diameter of 14 mm. The annular gap of about 15 cm, formed due to the excavation overcut, was filled under pressure with a bi-component grout.

Two tunnel sections (A and B) of the U5 were equipped with sensors to observe the development of normal forces and bending moments in the lining. The main instrumentation (Fig. 1) consisted of embedded strain sensors. In each monitored section, 13 vibrating wire transducers (VWT) and 26 strain gauges (SG) were positioned in the circumferential direction, and another 8 VWT in the longitudinal direction. At the VWT’s positions also the temperature was recorded. The lining’s deformations were measured to validate the strain measurement data. The amount of actual measurements in the sections was different. Therefore, for the analyses in this paper, only the better-equipped section B is considered. The measurements at both sections were initiated right after the ring assembly to register the complete loading history. Measurements at section B started in May 2021.

The geotechnical and structural situations of section B are shown in Fig. 1. The values of the soil parameters are given in section 4. Section B

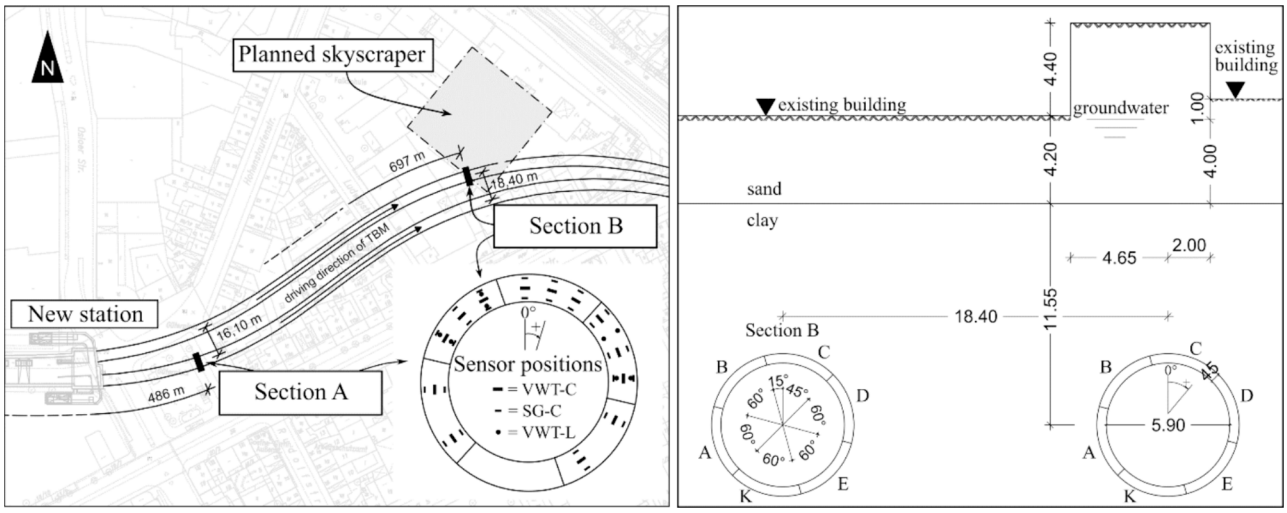

Fig. 1. U5 metro line. Left: overview of the eastern part of the U5 extension and instrumentation (VWT=vibrating wire transducer, SG=strain gauge, C=circumferential, L=longitudinal); right: the geotechnical and structural situation at section B, investigated in this study.

is surrounded by a Miocene clay layer, the so-called "Frankfurt Clay", which is overlain by a sand layer and is positioned below the groundwater table. At the time of this study, an old existing building is positioned on the ground surface. This building will later be demolished for the planned skyscraper. The axial distance between the two tubes is about 18.40 m, corresponding to 2.7 times the tunnel's outer diameter. It was measured that the interaction between the two tubes is small at this distance. This was also previously shown by studies of Do et al. (2014a). Therefore, in the subsequent calculations, only a single tube is simulated, neglecting the presence of the other one.

The development of the internal forces reaches a stable, final state with low changing rates after about one year of measurements (Fig. 2 and Fig. 3). Afterward, the internal forces remain relatively stable and are only slightly influenced by measurement inaccuracies and seasonal temperature effects. Therefore, for this study, the point in time corresponding to the final state was set to 365 days after the ring assembly.

The observed internal forces after 365 days at several positions along the tunnel's circumference at section B are shown in the right subfigures of Fig. 2 and Fig. 3, including a 95 percent error band that results, e.g., from the sensors' measurement inaccuracies. These values are used for the study presented in this paper.

The normal forces (Fig. 2) are quite regularly distributed. Values between −920 kN/m and −1200 kN/m (compression) are measured, with an average value ("normal force level") of −1010 kN/m. The bending moments (Fig. 3) fluctuate along the lining's circumference. The measured values range from 92 kN/m to −123 kN/m. Positive bending moments with positive tensile stresses at the intrados are found in the crown and negative bending moments with tensile stresses at the extrados at the side walls. This is expected for a tunnel in soft soil with a coefficient of lateral earth pressure k_0 smaller than one, as in this case. The tunnel invert was not equipped with sensors. The bending moment distribution is not exactly symmetric with respect to the vertical and horizontal axis but is slightly rotated clockwise according to the positions of the longitudinal joints in the segmental ring.

During the monitoring, not only the internal forces along (or tangential) to the lining's circumference ("tangential internal forces"), which are mainly addressed in this paper, were measured, but also the longitudinal normal forces in the direction of TBM advance (longitudinal tunnel axis) (see also Fig. 1). These forces, which are introduced into the lining by the thrust forces during tunnel construction, through friction cause an interaction of neighboring segments in the longitudinal direction that influences the structural behavior by increasing the

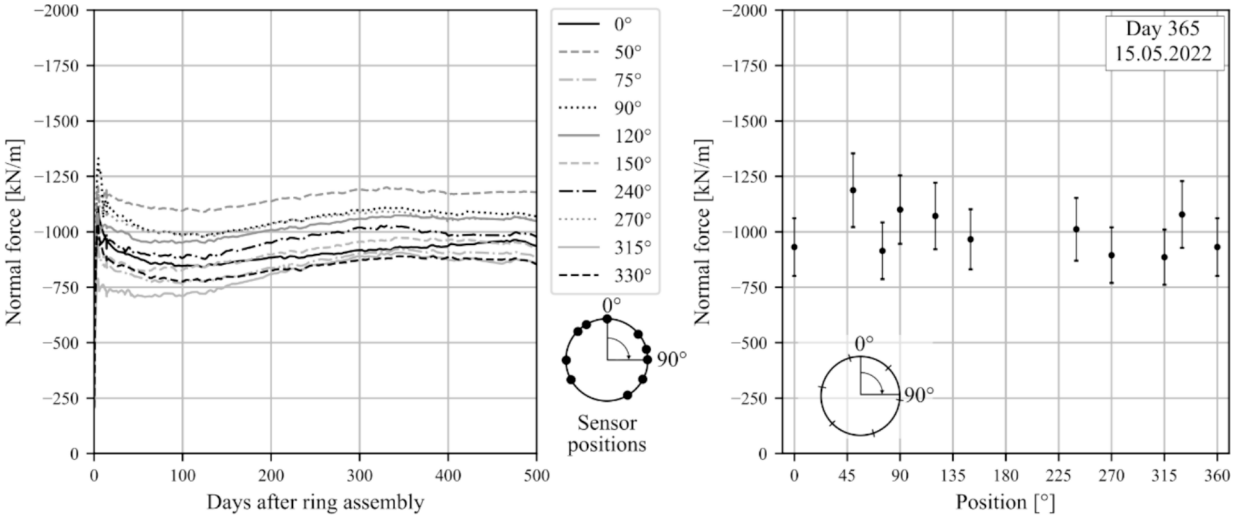

Fig. 2. Measured normal forces. Left: development over time starting right after ring assembly; right: normal forces distributed along the lining's circumference after 365 days with a 95 percent error band.

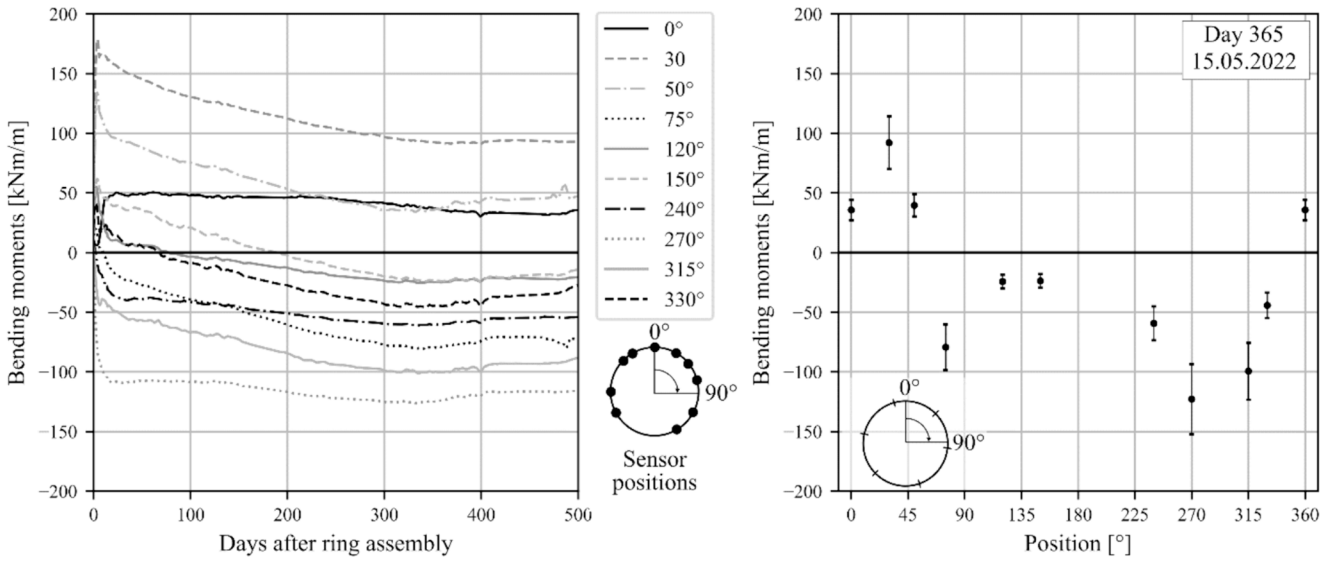

Fig. 3. Measured bending moments. Left: development over time starting right after ring assembly; right: bending moments distributed along the lining's circumference after 365 days with a 95 percent error band.

lining's stiffness. Their long-term behavior has been widely discussed in literature (e.g. Arnau et al., 2011; Gil Lorenzo, 2019). At U5, it was found that it is likely that the longitudinal forces (TBM jack induced) vanish during the tunnel's lifetime due to the long-term concrete behavior, creep and shrinkage, and temperature effects. This possibility is also pointed out in DAUB (2024) and DGGT (2014b). However, it remained unclear if the lining finds a new equilibrium before the longitudinal forces vanish and, therefore, if it "conserves" the early-stage effects of longitudinal ring coupling. Since it is unlikely, but not excluded, that longitudinal forces did not vanish or that a new equilibrium was found before the longitudinal forces vanished, the results of 3D models, including longitudinal ring interaction, are also considered in this study.

4. Developed calculation models and adopted modeling strategies

According to the geotechnical situation of the U5 metro tunnel and the findings during the monitoring campaign, a calculation model must, at minimum, explicitly include the effects of segmentation and the

Table 1
Characteristics of the developed models.

Model	Calculation method	Model dimensionality	Lining	Longitudinal joints	Soil constitutive model	Deconf. method	Soil-lining interaction
M1	Continuum model	2D, plane strain conditions	2D shell with real geometry	Interfaces[2] reproducing the moment-rotation relation of Janßen (1983)	Mohr-Coulomb [3]: lin.-elastic, perf.-plastic with yield function constant soil stiffness	CCM [5] with factor λ_r	Interfaces[2] with tensional cut-off [7]
M2		2D, plane strain, one longitudinal layer	One layer of 192 straight shell (2D) elements, assigned cross-section values	Rotational springs, reproducing the moment-rotation relation of Janßen (1983)	Hardening Soil [4]: stress-dep., elastoplastic suited for soft soil	SRM [6] with factor β_r	Single, connecting springs with tensional cut-off [7]
M3		3D ("pseudo 3D" [1]), with ten longitudinal layers and longitudinal ring interaction	As in Model M2, but ten layers		yield funct. of M.-Coul. different stiffnesses for loading, re-/unloading plastic deformations can occur before failure		
M4	Bedded beam model	2D, plane strain	96 straight beam (1D) elements with assigned cross-section values		–	–	Independent, non-linear springs with tensional cut-off
M5		3D ("quasi-3D"), two segmental rings incl. longitudinal ring interaction				–	

[1] see Fig. 5.
[2] set according to FLAC manual (2019) and Zaheri et al. (2020).
[3] seeMöller (2006).
[4] see Schanz et al. (1999).
[5] Convergence-confinement method.
[6] Stiffness-reduction method.
[7] By avoiding an unplanned load-bearing of the grout this prohibits unloading of the lining unwanted in structural design (DAUB 2024); assumption: grout stiffness exceeds soil stiffness (Behnen et al. 2013).

longitudinal joints, as well as groundwater effects, to predict final state internal forces. Due to the likely loss of longitudinal forces, a 2D model with plane strain conditions seems generally sufficient.

Five different models, M1 to M5 (Table 1) that consider these aspects and are in line with the mentioned state-of-the-art and, therefore, suitable for engineering practice were set up and are presented subsequentially. Their results are compared to the measurement data in section 5. For Model M1, the software package of FLAC 8.1 (Itasca, 2019), with a finite difference formulation (FDM), and for Model M2 to M5, the software package of Sofistik 2023 (Sofistik, 2023), with a finite element formulation (FEM), were used for this purpose.

4.1. General aspects and continuum models

All continuum models, M1, M2, and M3, include three main simulation steps: calculating the initial soil stress state under gravity, ground relaxation due to the excavation, and the lining installation and its loading. The effects of construction on ground relaxation are considered by two deconfinement methods (Table 1 and Fig. 4): the convergence-confinement-method (CCM) and the stiffness-reduction-method (SRM) (Do et al., 2014b; Do and Dias, 2017; Janin et al., 2015; Meschke, 2014). The CCM simulates ground relaxation through pressures σ_0, which counteract the excavated soil pressures and are reduced by $(1\text{-}\lambda_r)$ prior to lining installation and then removed. In the SRM, the soil stiffness E_s in the excavation area is reduced by β_r before removing the soil elements. Because shield-driven tunneling prevents major relaxations in the soil, the relaxation should not be set too high (e.g. Ahrens et al., 1982a; DAUB, 2014; DGGT, 2014b).

The soil layers are modeled according to Fig. 1, with the characteristics in Tables 1 to 3. The soil properties were available from the U5 geotechnical site report (CDM Smith, 2017). The effects of groundwater are included in the models. The concrete lining is modeled according to Tables 1 and 4 with a linear-elastic material law. In the models M2 to M5, the circular geometry is approximated with a sufficient number of straight elements, according to Ahrens et al. (1982a). Reinforcement has no significant effect in the expected stress range and is therefore neglected in this study.

The soil-lining interaction is modelled according to Table 1. As it is questionable if a significant tangential soil-lining interaction occurs due to the potentially low shear stiffness of the grout mortar and the low tangential bond between soil, grout, and lining (Ahrens et al., 1982a; Duddeck, 1980), the influence and the value of the tangential interaction are part of the study in this paper and addressed in the subsequent sections. Two cases are applied:

- "(Full) slip case" with no tangential interaction, as assumed e.g. by Schotte (2016) or Winselmann et al. (2000).
- "(Full) bond case" with full tangential interaction, as (additionally to the slip case) assumed e.g. by Arnau (2012), DAUB (2014), DGGT (2014b), and Kämper et al. (2016).

According to Möller (2006), the 2D model dimensions were chosen large enough to avoid an impact of the boundaries on the structural behavior of the tunnel itself. The distance between the tunnel invert and the bottom boundary is 31.7 m, and the distance between the horizontal boundaries is 70.0 m. Following sensitivity analyses, model M1 consisted of approximately 26,394 zones, model M2 of approximately 37,801 elements, and model M3 of approximately 377,626 elements.

In model M3 and model M5, additional interfaces occur in the ring joints, which are modeled according to Klappers et al. (2006), with prestressed, single springs at the positions of the packers and a tensional cut-off. The corresponding material parameters were available from the U5 structural design report (ARGE SBEV, 2017) and can be found in Table 4.

The required time for one calculation of the continuum model with the presented configuration can reach up to about 24 h, which is significantly more than for a bedded beam model, which is presented in the next section.

4.2. Additional specific aspects for bedded beam model

The bedded beam models M4 and M5 are set up according to Fig. 1 and Tables 1, 2, and 4. The general remarks from section 4.1 also apply to the bedded beam models. However, some additional, specific aspects are presented subsequently.

Fig. 6 shows a bedded beam model, similar to model M4. An angle of ± 45 degrees around the (shallow) tunnel crown remains unbedded (Ahrens et al., 1982a). In the bond case, tangential springs (not shown in Fig. 6) with a ratio of tangential to radial spring stiffness of 0.3 (e.g. Do, 2014; Plizzari and Tiberti, 2006; JSCE, 2007 as cited in ITA, 2019) are modeled perpendicular to the radial springs. In the slip case, a negligible tangential stiffness of 2.5 percent is applied to improve numerical stability (DAUB 2024). The active loading is set similarly as in ARGE SBEV (2017). In the bond case, also the tangential load components are applied. The corresponding calculation steps are shown in the Appendix. The (quasi-) 3D Model M5, respectively, consists of two equal rings that are coupled in the same way as in model M3. The segments are modeled with half of their real length.

The calculation time of a 2D or 3D bedded beam model is generally below 60 s and, therefore, significantly shorter compared to a continuum model.

4.3. Consideration of geometric imperfections

Next to the mentioned parameters, the assembly quality can also have an impact on the internal forces (Schotte, 2016). Therefore, a subsequent part of this paper includes considerations and calculations regarding the effects of geometrical assembly imperfections in longitudinal joints (Fig. 7) on internal forces. Their appearance is undoubted, and it has also been explicitly measured (Schotte et al., 2015; Schotte, 2016) that the ring assembly is not exactly perfect in many cases, which is the primary cause of longitudinal joint imperfections. In this paper, the effects of geometric imperfections are simulated for bedded beam models. The detailed development and validation of the applied

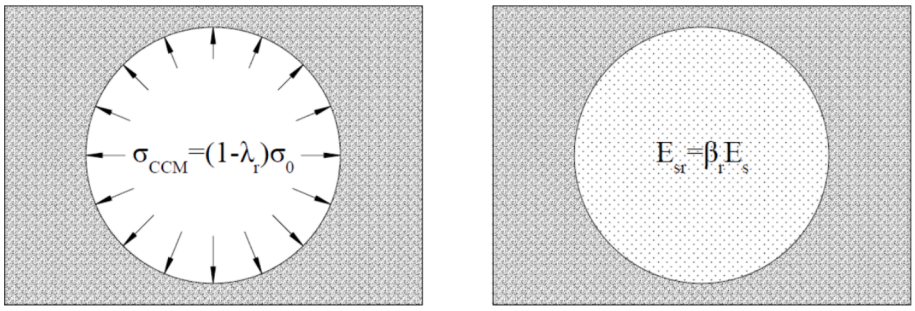

Fig. 4. Deconfinement methods and corresponding formulas. Left: the convergence confinement method (CCM); right: stiffness reduction method (SRM).

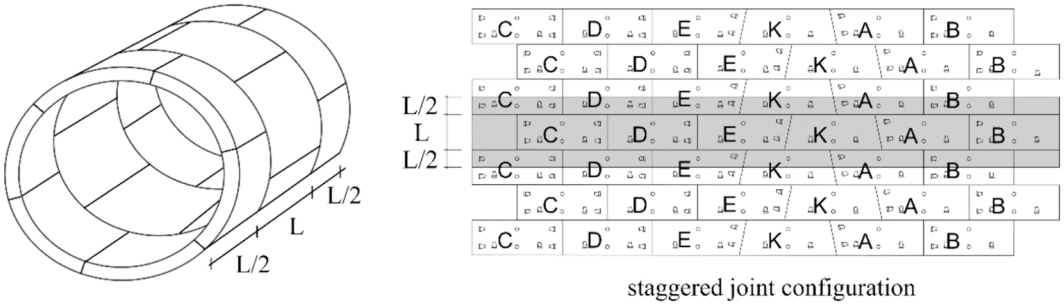

Fig. 5. „Pseudo-3D" model. Recurring cut-out of a segmental tunnel lining with staggered configuration with one whole plus two half segments in longitudinal direction.

Table 2
Soil parameters used in the numerical models.

Parameter	Clay (around the tunnel)		Sand (overlying layer)	
	Bandwidth from geotechn. report	Studied value(s)	Bandwidth from geotechn. report	Studied value(s)
Oedometric modulus E_s [MN/m^2] (primary loading / un-, reloading)	29—45[1] / 75	45[2], 75	60 / 120	60
Coefficient of lateral earth pressure k_0 [-]	0.57–0.75	– 0.58 (low) – 0.67 (medium) – 0.74 (high)	0.43	
Poisson Ratio [-]	0.4		0.35	
Dry density γ_{dry} [t/m^3]	1.27		1.97	
Saturated density γ_{sat} [t/m^3]	1.78		2.16	
Density under buoyancy γ' [t/m^3]	0.78		1.16	
Cohesion c [kN/m^2]	15–25	20	0	
Friction angle φ [°]	15–25	15, 20, 25	32.5 – 37.5	35
Dilation δ [°]	0		5	
Porosity [-]	0.52		0.19	
Permeability [m/s]	5e-8		1e-3	

[1] E_s = 45 MN/m^2 is the recommended value for structural design (bedded beam).
[2] used for bedded beam models.

Table 3
Parameters for the Hardening Soil constitutive model.

Parameter	Clay (around tunnel)	Sand (overlying layer)
$E_{50,ref}$ [MN/m^2]	35	50
$E_{oed,ref}$ [MN/m^2]	35	50
E_{ur} [MN/m^2]	105	125
m [-]	1.0	0.5
p_{ref} [kN/m^2]	100	100
ν_{ur} [-]	0.2	0.25

procedure to consider geometrical longitudinal joint imperfections is explained in Rauch and Fischer (2024b) and briefly summarized subsequently.

The effects of geometric joint imperfections are considered by modifying the moment-rotation-relation of Janßen (1983) (Fig. 7) for perfectly assembled longitudinal joints. In its original version, the moment-rotation-relation of Janßen (1983) simulates the opening of a longitudinal joint. An elastic material behavior is assumed, and the relation is reversible. To consider longitudinal joint imperfections due to

Table 4
Further specific calculation parameters.

Parameter	Value	Comment
Young's Modulus concrete C45 [N/mm2]	36,000	Determined through laboratory tests performed by the authors
Poisson ratio concrete	0.2	
Radial soil-lining interface [N/mm^3]	9000 for E_s = 45 MN/m^2 15,000 for E_s = 75 MN/m^2	For model M1 only
Radial soil-lining spring stiffness [kN/m^3]	1.1E6	For models M2 and M3 only
Longitudinal spring stiffness in ring joint [kN/m^3]	1.5E6	For models M3 and M5, acc. to Klappers et al. (2006) and ARGE SBEV (2017)
Shear spring stiffness in ring joint [kN/m^3]	0.6E6	For models M3 and M5, acc. to Klappers et al. (2006) and ARGE SBEV (2017)
Radial elastic spring stiffness [kN/m^3]	$= 1.0 * \frac{E_s}{R_m} =$ 14173	For models M4 and M5, for a shallow tunnel acc. to Duddeck (1980).

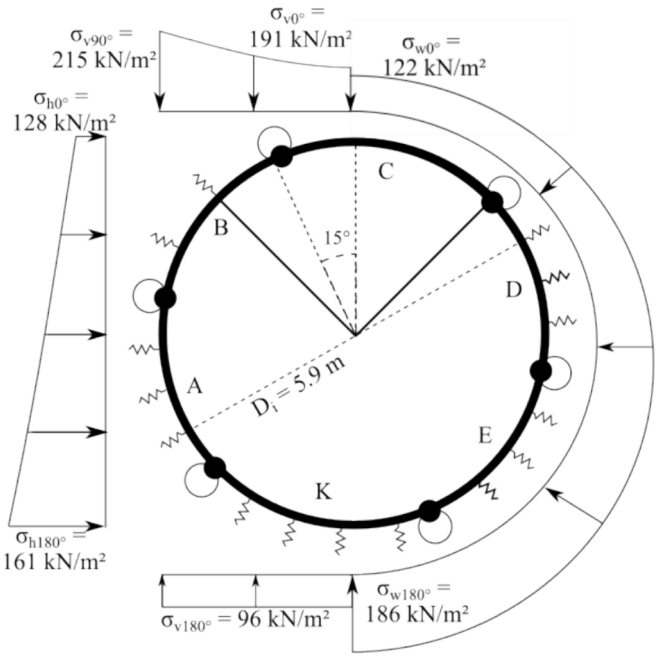

Fig. 6. Model M4. Geometry and applied active loading due to earth pressure, water pressure, and the old existing building loads on bedded beam model.

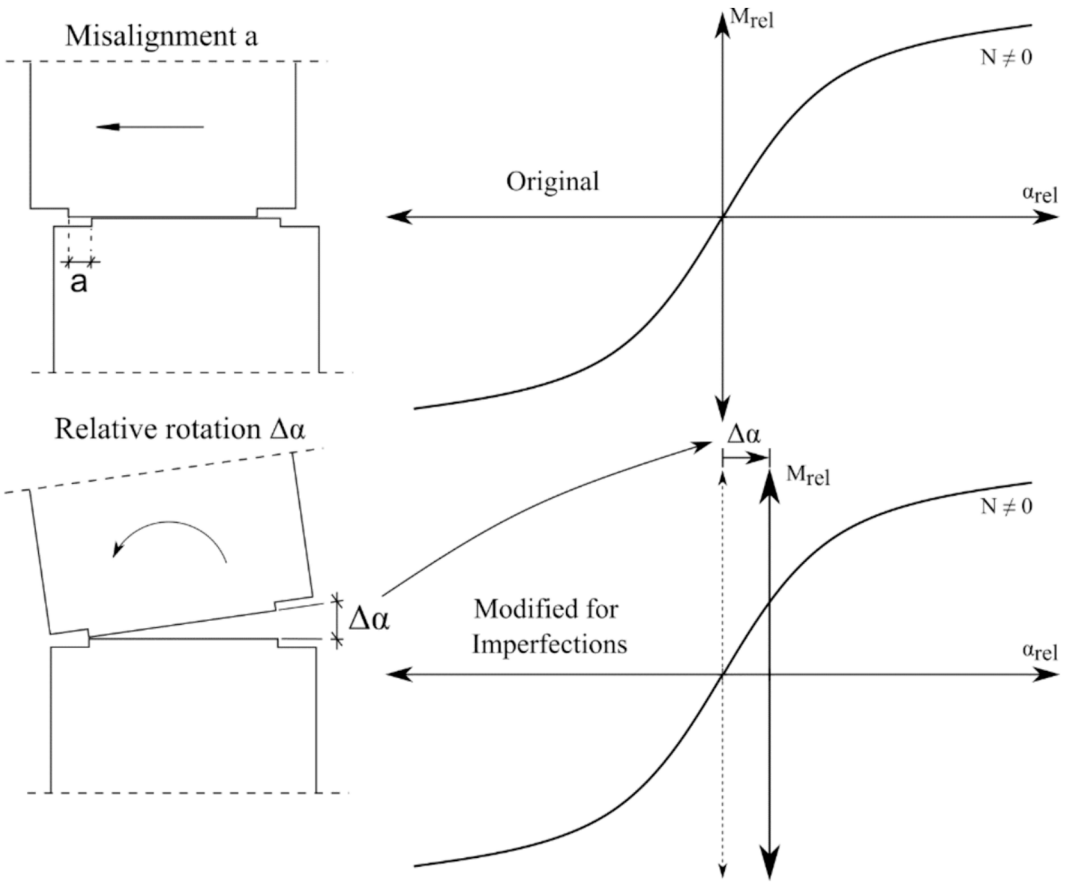

Fig. 7. Consideration of geometric longitudinal joint imperfections. Left: misalignment a, and relative rotation Δα between two adjoining segments; right: modification (bottom) of the original moment-rotation relation by Janßen (1983) for perfect assemblies (top) to simulate the effects of longitudinal joint imperfections; redrawn and modified from Rauch and Fischer (2024b).

assembly inaccuracies, the origin of the relation is moved by the magnitude of initial, imperfect joint openings $\Delta\alpha$ along the x-axis. Additional misalignments are neglected in this case. However, in a preliminary validation study, it was found that the influence of misalignments on the internal forces is small compared to rotational imperfections.

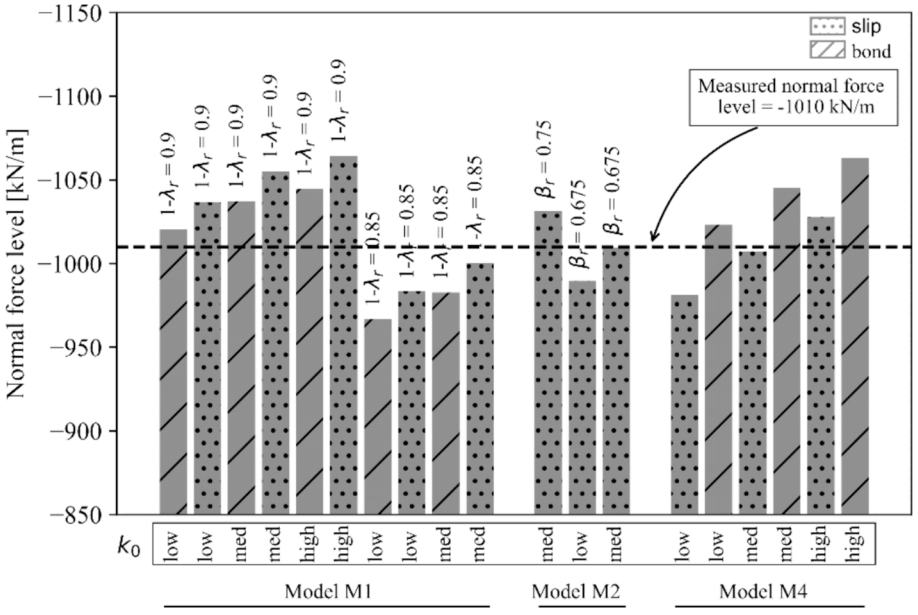

Fig. 8. Normal force levels. Obtained by the calculation models M1, M2 and M4 under the variation of: k_0, the parameters for ground relaxation and the tangential interaction case; and compared to in-situ measurements.

5. Comparison of calculated and measured internal forces

Subsequently, the agreements and differences between measurements and calculations regarding the internal forces in the stable, final state (365 days after ring assembly) are presented and discussed. The analysis is constructed step-by-step, descending from global to local, namely the normal force level, the normal force distribution, the peak bending moments and stresses, and the bending moment distributions.

5.1. Normal force level

The normal force level is the average of normal forces along the lining's circumference, giving an impression of the total loads borne by the lining. For the sake of comparability, the normal force level is not calculated along the full 360 degrees, but at the invert an angle of ± 30 degrees is excluded, as no sensors were placed there (see sensor positions in Fig. 2). The measured normal force level after 365 days was −1010 kN/m (negative in compression).

The calculation results of the models M1, M2, and M4 were considered for this analysis. Longitudinal ring coupling in the ring joints does not affect the normal force level, and therefore, the results of the models M3 and M5 are not shown. E_s was kept constant at 45 N/mm^2 in all calculations. Fig. 8 shows calculated normal force levels with good agreements compared to the measurement. The following can be noted:

- A good agreement between calculated and measured normal force levels can be found for reasonable and realistic parameter settings.
- The normal force level in the lining is – next to the overburden's weight, which is fixed in this study – most influenced by the parameters considering ground relaxation before excavation, which have to be chosen carefully. The available measurement data allows to calibrate them, which is done subsequently.
- Due to the analysis of bending moments that is shown later, k_0-values above the medium value of 0.67 will appear unlikely and are not further considered in the subsequent sections. For low to medium k_0-values (between 0.58 and 0.67) in model M1 with the CCM, a good agreement between 99.0 percent and 104.4 percent of measured and calculated normal force levels is found if $(1\text{-}\lambda_r)$ is between 0.85 and 0.90. This is slightly higher but close to the value of $(1\text{-}\lambda_r) = 0.8$, for which a good agreement between 2D and full-3D internal forces was found by Do and Dias (2017) for the final state. For model M2 with the SRM, the calculated values range between 98.0 and 99.9 percent of the measurements, if β_r is 0.675 or slightly higher. Due to this agreement, $(1\text{-}\lambda_r)$ is set to 0.85 and 0.90, and β_r to 0.675 in the subsequent sections.
- The normal force level of the model M4 also shows a good agreement with the measurements. The agreement is between 97.1 and 103.4 percent for low and medium k_0-values. Consequently, this supports the applied active loads, presented in section 4.2 and calculated in the Appendix.
- The impact of changing between the slip case and the bond case is stronger in the model M4 (bedded beam model) compared to model M1 (continuum model), and contrary. This is further discussed in section 6.

5.2. Normal force distribution

The measured normal force distribution is quite regular along the lining's circumference (Fig. 2). The calculation results of all models, M1 to M5, were considered to investigate the agreement between calculated and measured normal force distributions. Fig. 9 shows three calculation results with the best agreement to the measurements. All three apply the slip case and E_s = 45 N/mm^2. Quantitatively, the three corresponding rooted sums of squared errors are 160 (M1), 175 (M2), and 174 (M4). The grey area indicates the envelope of all calculation results. The analysis of the distributions yields the following results:

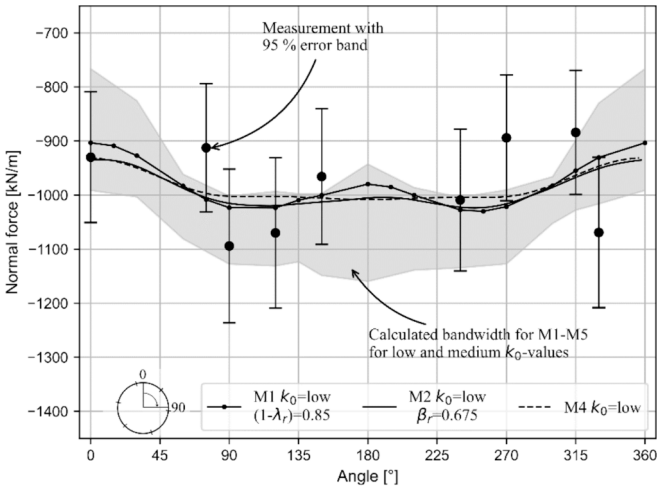

Fig. 9. Normal force distributions. Comparison of measured and calculated normal force distributions: measurements, three best-fitting calculation results (all slip cases and E_s = 45 N/mm^2) and bandwidth of all calculated normal force distributions (grey area).

- Generally, a good agreement between calculated and measured normal force distributions is found for almost all models with suited values for the ground relaxation parameters.
- The three best-fitting cases, obviously, also have a good agreement regarding the normal force levels: 97.3 percent (M1), 98.0 percent (M2), and 97.2 percent (M4).
- The best agreement is found for slip cases. Applying the bond case results in a stronger fluctuation of normal forces along the linings' circumference (not shown in Fig. 9). In the bond case, the absolute normal forces are lower in the crown and higher on the side walls. With the available data, it is not possible to address this topic definitely. However, the slightly better agreement for the slip cases is in line with other reports (e.g. Blom, 2002; DAUB, 2014; Schotte, 2016).
- No significant influence of the applied constitutive law for the soil is found.
- In the 3D models M3 and M5 (not shown in Fig. 9), contact forces are locally introduced in the ring joints at the positions of the packers. They influence the normal force distributions. However, these effects are moderate under the applied values of k_0 and E_s.

5.3. Peaks of bending moments and stresses

The peak bending moments and particularly the peak stresses are values of importance for the structural design. Calculation results of the models M1 to M5 are compared to the measured peak bending moments and peak stresses in tension (positive values) and in compression (negative). Different parameter configurations using the complete bandwidths (Table 2) are considered. The values for the ground relaxation parameters are set as in section 5.2. The results obtained and the measurement values are shown in Fig. 10 and Fig. 11. The following is found regarding the peak bending moments (Fig. 10):

- The measured peak bending moments are quite large compared to the calculations and cannot be reached with high k_0-values, as already mentioned previously. Only with low k_0-values it is possible to reach the measured peak bending moment, because, as expected, lower k_0-values lead to higher peak bending moments. In model M1 (slip case) changing from a medium to a low k_0-value increases the peak bending moment by 22.8 percent. The results of three variations of model M1 and one of model M5 exceed the measured peak

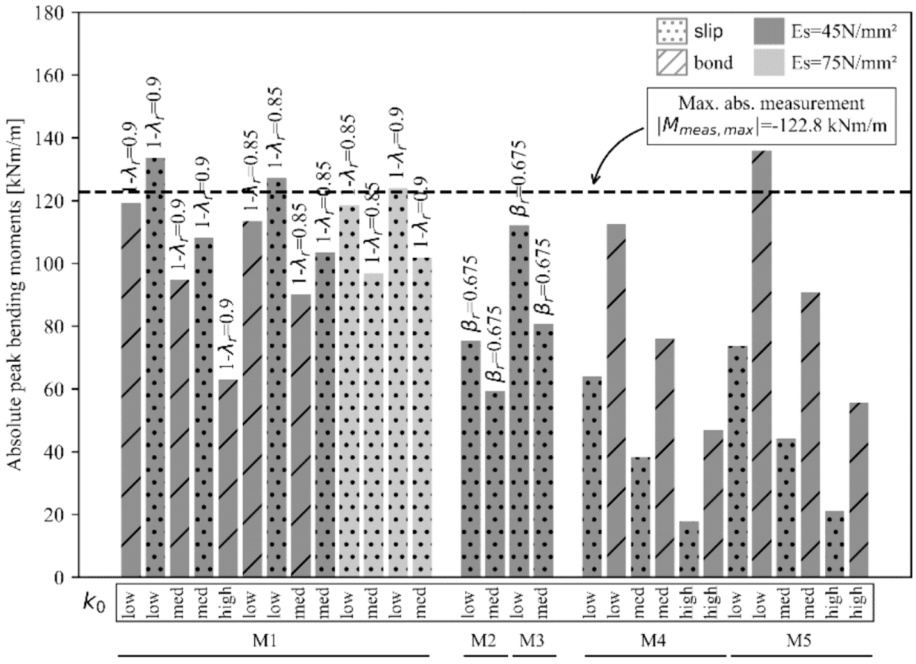

Fig. 10. Peak bending moments. Obtained by the calculation models M1 to M5 under the variation of: k_0, the parameters for ground relaxation, the longitudinal ring interaction and the tangential interaction case; and compared to in-situ measurements.

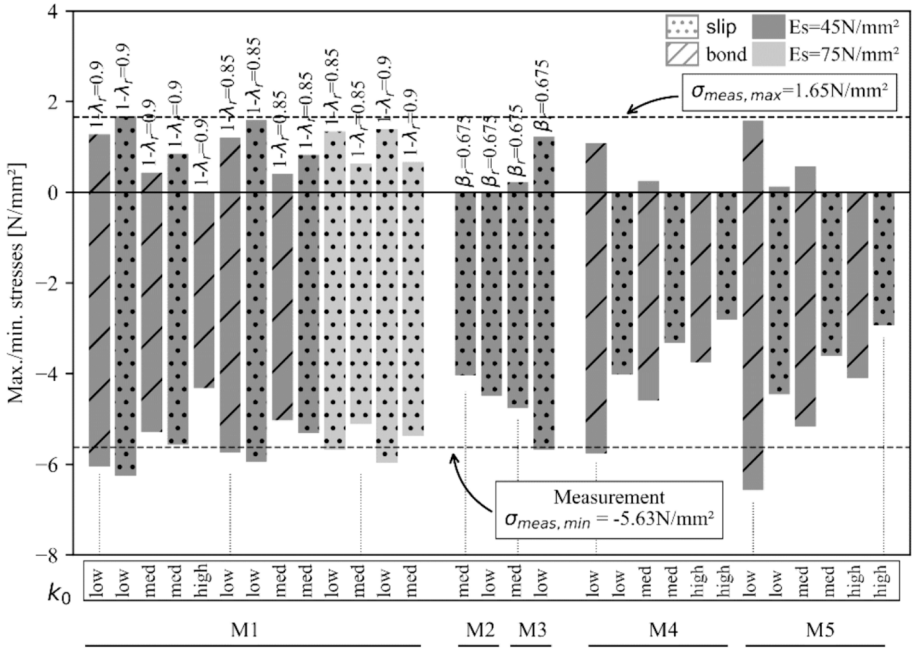

Fig. 11. Peak stresses. Obtained by the calculation models M1 to M5 under the variation of: k_0, the parameters for ground relaxation, the longitudinal ring interaction and the tangential interaction case; and compared to in-situ measurements. Positive values mean tension, negative values mean compression.

bending moments by a maximum of 8.9 percent. All the other studied models underestimate the actually measured peak bending moment.

- The 3D models M3 and M5 show increased peak bending moments compared to their 2D counterparts M2 and M4. This is due to the 3D longitudinal ring joint interaction, which leads to a stiffer system. The magnitude of the increase depends on the contact forces, which again depend on the possible/constraint deformations. In model M3, the peak is increased by 36.0 percent for a medium k_0 and by 48.7 percent for a low k_0 because lower k_0-values cause higher deformations.
- Next to the k_0-value and the longitudinal ring interaction, the selection of the constitutive law of the soil influences the peak bending moments. Linear-elastic laws, as in model M1 (where no limit stage is reached), M4, and M5, lead to increased peak bending moments. And in fact, the highest values are found for these models.
- To compare, the calculated peak bending moments of the three best-fitting models for the normal force distributions (Fig. 9) reach 103.2 percent (M1), 61.0 percent (M2) and 52.0 percent (M4) of the measured peak bending moments. This discrepancy is addressed in section 5.4.

The peak stresses are an indicator of the utilization ratio of the lining. It is, therefore, essential to predict them accurately enough. The analysis allowed the following observations regarding the agreement between calculated and measured peak stresses (Fig. 11):

- As expected, like the peak bending moments, higher stresses are found for lower k_0-values, in the case of 3D longitudinal ring interaction, with lower E_s, and for models with linear-elastic laws for the soil. In almost all cases the maximum stress values are found for the same models as at the peak bending moments.
- The calculated stresses barely reach the measured values. In tension, the highest stresses of 1.67 N/mm^2 are found for model M1 (slip case) with a low k_0-value, $E_s = 45$ N/mm^2, and $(1\text{-}\lambda_r) = 0.9$. In tension, this is the only model that reaches the maximum measured stresses of 1.65 N/mm^2. Generally, the highest tensional stresses are found for the models M1, M4, and M5 with a low k_0-value in the bond case. In many other calculations, no tension occurs.
- In compression, the highest calculated stresses of −6.57 N/mm^2 are found for model M5 (bond case) with a low k_0-value, exceeding the minimum observed stresses of −5.63 N/mm^2. Several other models also exceed this value, at maximum by 16.5 percent.

5.4. Bending moment distribution

As for the normal forces, the calculated bending moment distributions are compared to the measurements, which show fluctuating bending moments along the lining's circumference (Fig. 3). The same models and variations as in section 5.3 are investigated. Fig. 12 shows the obtained calculation results and the measured bending moment distribution. It includes the three calculated bending moment distributions with the best agreement compared to the measurements. The corresponding rooted sums of squared errors are 139 (both variations of M1) and 140 (M2). To summarize, the agreement between calculated and measured bending moment distributions is satisfying, but it is not as good as for the normal forces. In detail, the following observations are made:

- Qualitatively, all calculated distributions and the measurements are similar. Positive bending moments occur at the crown and the invert, while they are negative at the sidewalls. The distributions change signs four times.

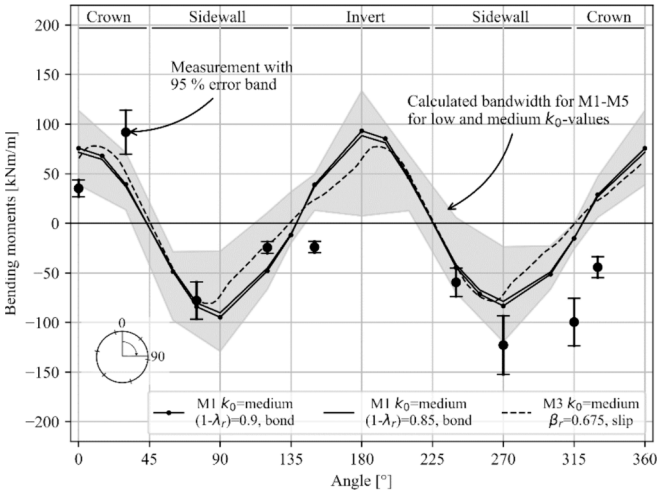

Fig. 12. Bending moment distributions. Comparison of measured and calculated bending moment distributions: measurements, three best-fitting calculation results (all $E_s = 45$ N/mm^2) and bandwidth of all calculated normal force distributions (grey area).

- Similar to the measurements, in most calculated distributions, the peaks are slightly rotated clockwise (not shown in Fig. 12). This is due to the positions of the longitudinal joints, which are not symmetrical to the vertical axis (Fig. 1).
- The three best-fitting models and parameter combinations in Fig. 12 (subsequently "M−best−fits") are not the same, that match the measured peak bending moments and stresses the best (see section 5.3). They neither are the calculation models with the best-fitting normal force distributions (subsequently "N-best-fits") (see section 5.2). Regarding the bending moment distribution, the "N-best-fits" reach a rooted sum of squared errors of 155, 149, and 166, which is only slightly worse compared to the "M−best−fits". On the other hand, regarding the normal force distributions, the "M−best−fits" reach rooted sums of squared errors of 290, 205, and 244, which is between 17 and 81 percent worse compared to the "N-best-fits". Consequently, the "N-best-fits" appear more reliable. Due to the lack of measurement data, it cannot be definitively excluded that the "M−best−fits" are realistic combinations. However, because of the elevated deviations in the normal force distributions, it seems likely that there might be an additional mechanism that has an (improving) impact on the agreement between calculated and measured bending moments. Consequently, this would improve the bending moment agreement of the "N-best-fits". This is discussed in the next section 5.5.
- Next to the three best-fitting models in Fig. 12, several further decently agreeing models are found that include longitudinal ring coupling (models M3 and M5, not shown). As mentioned in section 3, however, it is likely that the longitudinal forces will vanish with time and will not contribute to the structural behavior of the final stage. Nevertheless, even if they vanish, it is possible that through a new equilibrium that was established before, some of the effects of longitudinal joint coupling are "conserved" into the final state situation. Therefore, in any case, the agreement between calculations and measurement may be improved if longitudinal ring coupling is (partially) considered.

5.5. The effect of longitudinal joint imperfections

Although many different calculations were carried out, no (near-) "perfect" agreements were found between measurements and calculations. Normal forces have a very good agreement, while bending moments agree less. One reason therefore could be that up to this point only a perfectly circular lining following a perfect ring assembly was considered. Although it is common knowledge that assembly imperfections occur, assuming perfectly circular linings is the state-of-the-art, and it is not common to consider the effect of geometrical imperfections on the global internal forces explicitly. However, it is recommended to consider them for local situations, such as tensile splitting forces or partially concentrated compression stresses (DAUB 2024).

When longitudinal joint imperfections are introduced, the internal forces, particularly the bending moments, can change significantly. At U5 assembly imperfections were not measured explicitly. Therefore, potential values were determined by a back-analysis in order to analyze and illustrate their effects. The range of input values for the back-analysis was set considering limit values for assembly accuracy reported in guidelines and literature. Table 5 contains these limit values according to Baumann (1992), Cavalaro et al. (2011), DAUB (2024), ITA (2019), ÖVBB (2009), Schotte et al. (2015), and Schotte (2016).

Table 5
Considered limit values for assembly imperfections.

Parameter	Limit value
Misalignment	± 10 mm
Segment rotation	± 0.3°
Initial ovalization	0.5 percent of inner diameter

Additionally, the geometrical compatibility was checked in a geometrically realistic volume model to ensure that no overlapping occurred.

To visualize the effect of longitudinal joint imperfections on the internal forces, Fig. 13 shows the internal forces for three selected imperfect models M4, calculated with the method presented in section 4.3, compared to the results of a perfectly circular model M4 and the in-situ measurements at U5. In this case, a low k_0-value and the slip case were assumed.

Table 6 shows the corresponding geometrical configuration of the imperfect models. The following observations can be made:

- Geometrical longitudinal joint imperfections have no relevant influence on the normal forces.
- The imperfections significantly influence the bending moments due to the changed load introduction in the segments' longitudinal joints.
- Although the three imperfect models in Fig. 13 have different values of imperfections, they give similar results.
- The bending moment distribution agrees better with the measured distribution if longitudinal joint imperfections are considered. The rooted sum of squared errors is reduced from 167 for the perfectly circular model to values between 140 and 143 for the imperfect models.
- At U5, geometric imperfections were not measured. Therefore, only their general effects and relevance can be shown in this study. However, it should be noted that considering longitudinal joint imperfections leads to higher (global) stresses within the lining. In the case of Fig. 13, stresses in compression are increased by 26.2 to 33.9 percent if imperfections of Table 6 are considered. On the other hand, tensional stresses appear in the imperfect models which is not the case for the perfectly circular model. Therefore, this may be relevant for structural design, and a more extensive study on the relevance of longitudinal joint imperfections will be carried out and published later.

6. Continuum models vs. Bedded beam models

When comparing the results of the applied calculation models to each other, it can be observed that the calculation results of continuum models and bedded beam models are not equal – because, in fact, the models and their approaches are different, e.g., regarding load application and soil-lining interaction. From the calculation results presented in section 5, the following can be noted:

- All models give quite similar results for the normal forces.
- In the case of the shallow U5, the results of model M1, on average, give the highest stresses. However, the peak stresses are reached with model M5, which is why the bedded beam models would consequentially be relevant for design here (Fig. 11). However, this is only the case for low k_0-values and could, therefore, be inverted under different boundary conditions. It appears impossible to define a-priori, which model will give the most conservative results. In Fig. 11, it can also be observed that while the stress peaks of models M1, M2, and M3 are quite similar, the differences between the stress peaks of different models M4 and M5 are larger. This is attributed to the fact that bedded beam models depend on fewer parameters and are, therefore, more sensitive to parameter changes. Consequently, it might be recommendable to consider wider parameter bandwidths when using bedded beam models, and contrarily, it seems likely that if there is less knowledge of the tunnel's boundary conditions, the bedded beam models will give more conservative results due to the broader considered bandwidth. This should, however, be investigated in further studies.
- Bedded beam models and the resulting internal forces are more sensitive to changes of k_0-values, which are a key calculation parameter. On average, the peak stresses change by 18.2 percent in model M1 and by 22.3 percent in model M4 if the k_0-value is modified.
- The biggest difference is found regarding the tangential soil lining interaction (slip and bond). While in continuum models the slip cases give slightly higher peak moments and stresses (on average by 8.0 to 11.0 percent), it is the opposite for the bedded beam models (the magnitudes can more than double). This difference is likely due to the differing load application and possible redistributions in the continuum models. Such redistributions cannot occur in the bedded beam models (Behnen et al., 2013), and therefore, the tangential components are simply not applied. Consequently, when using bedded beam models, the bond cases should be considered.

From the analyses in this paper, definitively answering the question of which model is more "realistic" is difficult. However, it should be remembered that the concept and the formulas for bedded beam models were derived from continuum models for deep tunnels and then adapted to shallow tunnels (Ahrens et al., 1982a). Consequently, and also because of the higher degree of detailing, it is justifiable to assume that continuum models are more realistic. This is supported by the findings shown in section 5, in which continuum models, in some cases, gave a slightly better agreement to the in-situ measurements. However, it should be considered that further modeling strategies exist within continuum models (and also within bedded beam models) that might have a different agreement. Nevertheless, bedded beam models still have some advantages on their side: the soil parameters required for bedded beam models are determined more easily (Ahrens et al., 1982b), and the calculation time is much lower, which is an advantage in parametric studies, which – also following the findings here – should be part of any tunnel design.

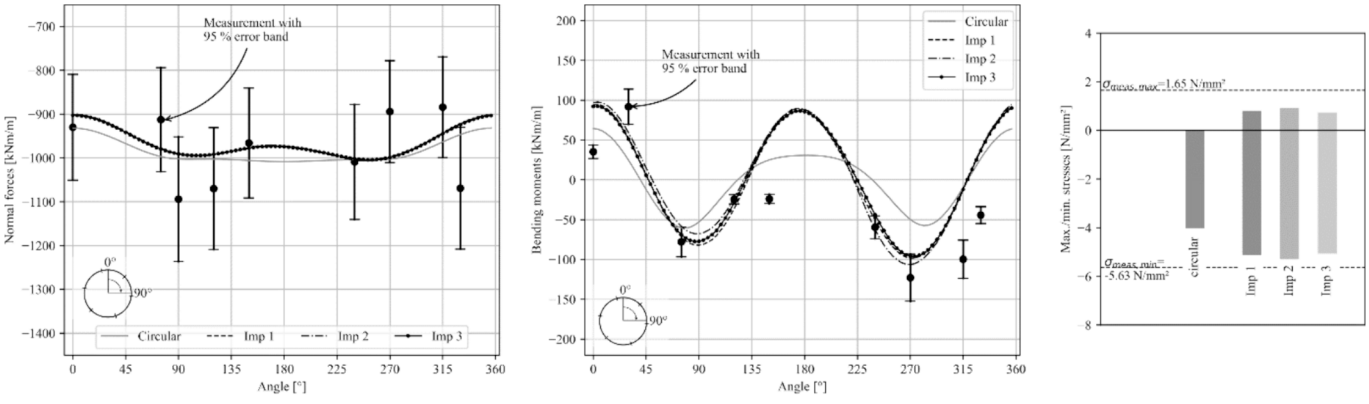

Fig. 13. Effect of geometrical longitudinal joint imperfections: on normal forces (left), bending moments (center) and stresses (right) for three imperfect models M4 compared to a perfectly circular model M4 and the measurements.

Table 6
Applied geometric configurations of imperfect models: rotations of segments and misalignments of longitudinal joints.

Model	Segment rotations [°]						Joint misalignment [mm]					
	A	B	C	D	E	K	A/B	B/C	C/D	D/E	E/K	K/A
Imp 1	0.087	0.068	0.024	0.085	0.168	−0.017	2.9	4.1	2.5	1.9	1.1	0.1
Imp 2	−0.088	−0.011	−0.048	0.039	−0.046	−0.085	2.1	7.8	0.8	5.0	3.2	9.9
Imp 3	−0.15	0.010	0.066	−0.067	−0.069	0.066	1.6	7.6	1.6	3.4	2.8	8.3

7. Conclusions

Five different calculation models, three continuum models and two bedded beam models, with several different state-of-the-art modeling strategies and various, realistic parameter combinations were applied to the case of the newly built segmental tunnel lining of the extension of the U5 metro line in Frankfurt (Main), Germany. This paper compares their calculated final state internal forces to in-situ measured internal forces at the U5.

A good agreement between measurements and calculations can be found for the normal forces for many different models. Although the general agreement is worse for the bending moments, the agreement is satisfying for some models with suited parameter combinations. Their measured qualitative distribution can be reproduced well in calculations, while the quantitative comparisons show some differences. In many cases, the calculated peak bending moments stay below the measurements. This also holds for the lining's stresses. However, some parameter combinations – sometimes at the edge of the possible realistic parameter bandwidth – give calculated stress magnitudes similar to the measurements.

When calculating global internal forces, a perfectly circular lining, without geometric assembly imperfections, is mostly assumed in structural analyses. It was shown, however, that taking geometric imperfections under consideration has a significant effect on the internal forces, particularly on the bending moments, and can lead to an improved agreement between calculations and measurements.

Finally, the following conclusions can be drawn regarding the applied calculation models for their applicability in the engineering practice:

- Generally, when considering the possible parameter bandwidth, all studied state-of-the-art calculation methods can give the results relevant for structural design with an acceptable accuracy.
- From the findings presented in this paper, it seems likely that continuum models give more realistic results compared to bedded beam models for the investigated type of shallow tunnel. However, it is difficult to determine a priori which model configuration and parameter combination will give the most realistic results. Consequently, parametric studies that cover the possible realistic bandwidths of relevant geotechnical parameters are essential. To enable this with reasonable effort, calculation times should be low enough. The latter favors smaller models over larger three-dimensional models. Following this, it appears recommendable to use 2D and pseudo-3D continuum models in structural design for situations and boundary conditions similar to those studied in this paper (e.g. final-state, no local geometry or load changes as cross-passages, no interactions with neighboring linings, shallow tunnel etc.).
- The ratio of lateral to vertical earth pressure k_0 is probably the most relevant parameter for calculations in structural design. The potential bandwidth, particularly below medium values, should be included carefully in the parametric study. Moreover, in continuum models, the constitutive model for the soil should be selected carefully. Applying the Mohr-Coulomb model with a linear-elastic, perfectly plastic behavior mostly led to more conservative results compared to the Hardening Soil model.
- It remained unsolved to which extent (early-stage) 3D longitudinal ring coupling, in reality, influences the final state internal forces. Since longitudinal ring coupling can have a significant impact on the lining's stresses the effects of ring coupling should be included in the parametric studies for structural design, e.g. by pseudo-3D calculations. The same holds for the tangential interaction. Therefore, both the slip cases and the bond cases should be studied, particularly when using bedded beam models. Focus on these two parameters should also be part of future measurements and investigations.

It was also shown that neglecting the effects of geometric imperfections on the internal forces leads to non-conservative and probably less realistic results. Further studies will address this topic and investigate if, under which boundary conditions and how such geometric imperfections should be explicitly considered in structural design. For future measurement campaigns, it is recommended to explicitly measure geometric imperfections during and after assembly.

CRediT authorship contribution statement

Fabian Rauch: Writing – original draft, Visualization, Validation, Software, Methodology, Investigation, Data curation, Conceptualization. **Pierpaolo Oreste:** Writing – review & editing, Visualization, Validation, Supervision, Software, Methodology, Investigation, Conceptualization. **Oliver Fischer:** Visualization, Validation, Supervision, Investigation, Funding acquisition, Conceptualization.

Declaration of competing interest

The authors declare that they have no known competing financial interests or personal relationships that could have appeared to influence the work reported in this paper.

Data availability

No data was used for the research described in the article.

Acknowledgements

The structural monitoring project at the U5 metro line in Frankfurt (Main), Germany, was commissioned by "Stadtbahn Entwicklung und Verkehrsinfrastrukturprojekte Frankfurt GmbH (SBEV)", a subsidiary of "Stadt Frankfurt am Main" and "VGF—Verkehrsgesellschaft Frankfurt". The authors also want to thank Dipl.-Ing. Christoph Klappers of ZPP Ingenieure AG and Dipl.-Ing. Gereon Behnen of Büchting + Streit AG, who gave significant input to create the applied models.

Appendix:. active loading on bedded beam models

Fig. 6 shows the bedded beam model's geometry and (active) loading. The active loading is set similarly as in ARGE SBEV (2017), and its calculation is presented subsequently.

The vertical earth pressure is calculated according to the geotechnical situation of Fig. 1 and the specific weight of the soil layers (Table 2). Because of the shallow position, the complete overburden is applied as an active load. Exemplarily, the loads are calculated in Equations 1 to 11 for a k_0-value of 0.58 (low). To account for buoyancy and the unloading due to excavation (parameter B in Equation (4), a reduced vertical earth pressure σ_v is applied to the lower half of the lining as in ARGE SBEV (2017). The horizontal earth pressure σ_h is calculated by multiplying the non-reduced vertical earth pressure σ_v by k_0. The earth pressure is then split into a radial and a tangential component. While the radial component is always applied, the tangential component is applied depending on the case (slip/bond), as the loading situation must be compatible with the bedding (Behnen et al., 2013). The water pressure σ_w always only acts radially.

$$\sigma_v = \sigma_{v,building} + \gamma_{sand,dry} * h_1 + \gamma'_{sand} * h_2 + \gamma'_{clay} * h_3 \tag{1}$$

$$\sigma_{v,0^\circ} = 75\,kN/m^2 + 19.3\frac{kN}{m^3} * 0.4\,m + 11.4\frac{kN}{m^3} * 3.8m + 7.7\frac{kN}{m^3} * 8.425\,m = 190.9\,kN/m^2 \tag{2}$$

$$\sigma_{v,90^\circ} = 190.9\,kN/m^2 + 7.7\frac{kN}{m^3} * 3.175\,m = 215.4\,kN/m^2 \tag{3}$$

$$\sigma_{v,180^\circ} = \sigma_{v,0^\circ} - B = \sigma_{v,0^\circ} - \frac{A_{out} * \gamma_w + A_{out} * \gamma'_{clay}}{D_{out}} = 190.9\frac{kN}{m^2} - \frac{36.3m^2 * \left(10\frac{kN}{m^3} + 7.7\frac{kN}{m^3}\right)}{6.8} = 96.4\,kN/m^2 \tag{4}$$

$$\sigma_{h,0^\circ} = \sigma_{v,0^\circ} * K_0 = 190.9\frac{kN}{m^2} * 0.67 = 127.9\,kN/m^2 \tag{5}$$

$$\sigma_{h,180^\circ} = (\sigma_{v,0^\circ} + D * \gamma'_{clay}) * K_0 = (190.9\frac{kN}{m^2} + 6.35\,m * 7.7\,kN/m^3) * 0.67 = 160.7\,kN/m^2 \tag{6}$$

$$\sigma_{w,0^\circ} = 10\frac{kN}{m^3} * (3.8\,m + 8.425\,m) = 122.25\,kN/m^2 \tag{7}$$

$$\sigma_{w,180^\circ} = 10\frac{kN}{m^3} * (3.8\,m + 8.425\,m + 2 * 3.175\,m) = 185.75\,kN/m^2 \tag{8}$$

References

ACI, 2020. Guide for Precast Concrete Tunnel Segments (ACI Committee 533). ACI American Concrete Institute.

Ahrens, H., Lindner, E., Lux, K.H., 1982a. Zur Dimensionierung von Tunnelausbauten nach den "Empfehlungen zur Berechnung von Tunneln im Lockergestein (1980). Die Bautechnik. 59 (8), 260–273.

Ahrens, H., Lindner, E., Lux, K.H., 1982b. Zur Dimensionierung von Tunnelausbauten nach den "Empfehlungen zur Berechnung von Tunneln im Lockergestein (1980)" Fortsetzung. Die Bautechnik. 59 (9), 303–311.

Arnau, O., Molins, C., 2012. Three-dimensional structural response of segmental tunnel linings. Eng. Struct. 44, 210–221. https://doi.org/10.1016/j.engstruct.2012.06.001.

Arnau, O., Molins, C., Blom, C.B.M., Walraven, J.C., 2011. Longitudinal time-dependent response of segmental tunnel linings. Tunn Undergr Sp Tech. 28 (1), 98–108. https://doi.org/10.1016/j.tust.2011.10.002.

Arnau, O., 2012. Structural Response of Precast Concrete Segmental Tunnel Linings. Universitat Politecnica de Catalunya, Barcelona: Dissertation.

Bakhshi, M., Nasri, V., 2014a. Guidelines and Methods on Segmental Tunnel Lining Analysis and Design - Review and Best Practice Recommendation. Proceedings of the World Tunnel Congress, Iguassu Falls.

Bakhshi, M., Nasri, V., 2014b. Design Considerations for Precast Tunnel Segments According to International Recommendations, Guidelines and Standards. TAC 2014, Vancouver.

Baumann, T., 1992. Tunnelauskleidungen mit Stahlbetontübbingen. Die. Bautechnik 69 (1), 11–20.

Behnen, G., Nevrly, T., Fischer, O., 2013. Bettung von Tunnelschalen. In: Laackmann, K., Balthaus, H., Wittke-Schmitt, B. (Eds.), Taschenbuch Für Den Tunnelbau 2013. VGE Verlag, Essen, pp. 235–282.

Behnen, G., Nevrly, T., Fischer, O., 2015. Soil-structure interaction in tunnel lining analyses. Geotechnik 38 (2), 96–106. https://doi.org/10.1002/gete.201400010.

Blom, C.M.B., 2002. Design philosophy of concrete linings for tunnels in soft soils. TU Delft, Delft: Dissertation.

BMVI, 2022. Zusätzliche Technische Vertragsbedingungen und Richtlinien für Ingenieurbauten. Bundesministeriums für Digitales und Verkehr (BMVI).

Bobylev, N.G., Guo, D., Benardos, A., 2023. Urban underground space use in a climate neural city. Athens, Greece: Proceedings of the WTC 2023, 9–13. https://doi.org/10.1201/9781003348030-2.

Budach, C., Kulkarni, R., Weiner, T., Kirchner, S., 2020. Geotechnische und tunnelbautechnische Aspekte beim Bau der U5 in Frankfurt am Main. Geotechnik 43 (4), 283–288. https://doi.org/10.1002/gete.202000028.

Cavalaro, S.H.P., Blom, C.B.M., Walraven, J.C., Aguado, A., 2011. Structural analysis of contact deficiencies in segmented lining. Tunn Undergr Sp Tech. 26 (6), 734–749. https://doi.org/10.1016/j.tust.2011.05.004.

DAUB, 2014. Recommendations for the design, production and installation of segmental rings. Deutscher Ausschuss für unterirdisches Bauen (DAUB).

DAUB, 2024. Recommendations for the design, production and installation of segmental rings. Deutscher Ausschuss für unterirdisches Bauen (DAUB).

DB-Netze, 2014. Richtlinie 853 - Eisenbahntunnel planen, bauen und instand halten. DB Netz AG.

DGGT, 2014a. Empfehlungen des Arbeitskreises "Numerik in der Geotechnik" – EANG. Ernst & Sohn, Berlin, pp. 77-97.

DGGT, 2014b. Empfehlungen des Arbeitskreises "Numerik in der Geotechnik" – EANG. Ernst & Sohn, Berlin, 1-36.

Do, N.A., Dias, D., 2017. A comparison of 2D and 3D numerical simulations of tunnelling in soft soils. Environ. Earth Sci. 76 (3), 1–12. https://doi.org/10.1007/s12665-017-6425-z.

Do, N.A., Dias, D., Oreste, P., Djeran-Maigre, I., 2014a. 2D numerical investigations of twin tunnel interaction. Geomech Eng. 6 (3), 263–275. https://doi.org/10.12989/gae.2014.6.3.263.

Do, N.A., Dias, D., Oreste, P., Djeran-Maigre, I., 2014b. 2D tunnel numerical investigations: the influence of the simplified excavation method on tunnel behaviour. Geotech. Geol. Eng. 32, 43–58. https://doi.org/10.1007/s10706-013-9690-y.

Do, N.A., 2014. Numerical Analyses of Segmental Tunnel Lining under Static and Dynamic Load Analyses. University of Grenoble, Grenoble: Dissertation.

Duddeck, H., 1980. Empfehlungen zur Berechnung von Tunneln im Lockergestein. Die Bautechnik. 57 (10), 349–356.

Fischer, O., Nevrly, T., Behnen, G., 2014. Fertigteile im Tunnelbau. In: Bergmeister, K., Fingerloos, F., Wörner, J.D. (Eds.), Betonkalender 2014. Ernst & Sohn, Berlin, pp. 233–302. https://doi.org/10.1002/9783433603352.ch8.

FLAC manual, 2019. Itasca Consulting Group, Manual FLAC - Fast Lagrangian Analysis of Continua: 3. Interfaces.

Gil Lorenzo, S., 2019. Thermally-induced longitudinal decompression of simultaneously backfill grouted tunnels. Tunn Undergr Sp Tech. 91. https://doi.org/10.1016/j.tust.2019.103022.

Grübl, F., 2012. Segmental Ring Design: New Challenges with High Tunnel Diameters. World Tunnel Congress 2012, Bangkok.
ITA, 2019. Guidelines for the Design of Segmental Tunnel Linings. International Tunnelling Association, Working Group 2.
Itasca Consulting Group, 2019. FLAC - Fast Lagrangian Analysis of Continua, Ver. 8.1 Minneapolis: Itasca.
Janin, J.P., Dias, D., Emeriault, F., Kastner, R., Le Bissonnais, H., Guilloux, A., 2015. Numerical back-analysis of the southern Toulon tunnel measurements: a comparison of 3D and 2D approaches. Eng. Geol. 195, 42–52. https://doi.org/10.1016/j.enggeo.2015.04.028.
Janßen, P., 1983. Tragverhalten von Tunnelausbauten mit Gelenktübbings. TU Braunschweig, Braunschweig: Dissertation.
JSCE, 2007. Japanese Railway Technical Research Institute. Standard Specifications for Tunneling – 2006: Shield Tunnels.
Kämper, C., Putke, T., Zhao, C., Lavasan, A.A., Barciaga, T., Mark, P., Schanz, T., 2016. Vergleichsrechnungen zu Modellierungsvarianten für Tunnel mit Tübbingauskleidung. Bautechnik 93 (7), 421–432. https://doi.org/10.1002/bate.201500064.
Klappers, C., Grübl, F., Ostermeier, B., 2006. Structural Analyses of segmental lining - coupled beam and spring analyses versus 3D-FEM calculations with shell elements. Tunn Undergr Sp Tech. 21 (3–4), 254–255. https://doi.org/10.1016/j.tust.2005.12.116.
Kolymbas, D., 2008. Tunnelling and Tunnel Mechanics. Springer, Berlin, pp. 367–377.
Leonhardt, F., Reimann, H., 1966. Betongelenke. Der Bauingenieur. 41, 2.
Marwan, A., Gall, V.E., Alsahly, A., Meschke, G., 2021. Structural forces in segmental linings: process-oriented tunnel advance simulations vs. conventional structural analysis. Tunn Undergr Sp Tech. 111. doi: 10.1016/j.tust.2021.103836.
Marwan, A., 2019. Computational Analysis of Segmental Linings in Mechanized Tunneling. RUB, Bochum: Dissertation.
Meschke, G., Breitenbücher, R., Freitag, S., König, M., Thewes, M., 2023. Interaction modeling in mechanized tunneling. Springer Nature, Cham. https://doi.org/10.1007/978-3-031-24066-9.
Meschke, G., 2014. Numerik im Tunnelbau, in: Bergmeister, K., Fingerloos, F., Wörner, J. D. (Eds.), Betonkalender 2014. Ernst & Sohn, Berlin, pp. 233–302. doi: 10.1002/9783433603352.ch7.
Möller, S., 2006. Tunnel induced settlements and structrual forces in linings. Universität Stuttgart, Stuttgart: Dissertation.
Oreste, P., 2007. A numerical approach to the hyperstatic reaction method for the dimension of tunnel supports. Tunn Undergr Sp Tech. 22, 185–205. https://doi.org/10.1016/j.tust.2006.05.002.
ÖVBB, 2009. Richtlinie Tübbingsysteme aus Beton. Österreichische Vereinigung für Beton und Bautechnik.
Plizzari, G., Tiberti, G., 2006. Steel fibers as reinforcement for precast tunnel segments. Tunn. Undergr. Space Technol.
Rauch, F., Fischer, O., 2023. Long-term structural behavior of inner-city segmental tunnel linings investigated by an innovative structural monitoring. Proceedings of the World Tunnel Congress 2023, Athens, 2510–2518. doi: 10.1201/9781003348030-302.
Rauch, F., Fischer, O., 2024b How to Consider the Effects of Longitudinal Joint Imperfections on Internal Forces in Segmental Tunnel Linings. Proceedings of the World Tunnel Congress 2024, Shenzhen. doi: 10.1201/9781003495505-43.
Rauch, F., Fischer, O., 2022. Structural monitoring of segmental tunnel linings: towards safer and more resource efficient tunnels. Civil Engineering Design. 7 (1–3), 62–71. https://doi.org/10.1002/cend.202100053.
Rauch, F., Fischer, O., 2024. Structural behavior of a segmental tunnel lining based on in situ measurements. J Perform Constr Fac. 38, 4. https://doi.org/10.1061/JPCFEV/CFENG-4688.
Sauer, J., 2016. Ökologische Betrachtungen zur Nachhaltigkeit von Tunnelbauwerken der Verkehrsinfrastruktur. TUM, Munich: Dissertation.
Sbev, A.R.G.E., 2017. Static Report / Standsicherheitsnachweise - Stadtbahnstrecke B, Teilabschnitt 3 Europaviertel Tübbingtunnel. ARGE Stadtbahn Europaviertel, Frankfurt.
Schade, T., Iffländer, R., Langmaack, L., Uhlman, D., 2023. Frankfurt U5 metro extension - the challenging high pressure inner city project. Proceedings of the WTC 2023, Athens, 2228–2236. doi: 10.1201/9781003348030-268.
Schanz, T., Vermeer, P.A., Bonnier, P.G., 1999. The hardening soil model: Formulation and verification. Beyond 2000 in Computational Geotechnics - 10 years of PLAXIS. Balkema, Rotterdam.
Schotte, K., De Wulf, A., Van Bogaert, P., De Backer, H., 2015. Quantification of Installation Inaccuracies and their Effect on the Design of Segmental Tunnel Linings. Proceedings of ISEC 2015: Implementing Innovative Ideas in Structural Engineering and Project Management, 921–926.
Schotte, K., 2016. Verification of the Performance of Segmental Tunnel Linings Using Strain and Ovalisation Monitoring. University of Gent, Gent: Dissertation.
Smarslik, M., Putke, T., Marwan, A., Gall, V.E., Meschke, G., Mark, P., 2017. Berechnungsmodelle für Bau- und Endzustände von Tübbingtunneln,.in: Laackmann, K., Balthaus, H., Wittke-Schmitt, B. (Eds.), Taschenbuch für den Tunnelbau 2018. Ernst & Sohn, Berlin.
CDM Smith, 2017. Geotechnical Report/Geotechnisches Gesamtgutachten - Zusammenfassende Darstellung der Baugrund- und Grundwasserverhältnisse (Stadtbahnbau, Grundstrecke B, Teilabschnitt 3 - Europaviertel. Frankfurt.
Sofistik, 2023. Sofistik: Service Pack 2023, Nürnberg. Sofistik AG, Germany.
Thewes, M., 2014. Tunnelbau im Schildvortrieb – Verfahrenstechnik und Planungsgrundlagen, in: Bergmeister, K., Fingerloos, F., Wörner, J.D. (Eds.), Betonkalender 2014. Ernst & Sohn, Berlin, pp. 233–302. doi: 10.1002/9783433603352.ch6.
Winselmann, D., Städing, A., Babendererde, L., Holzhäuser, J., 2000. Aktuelle Berechnungsmethoden für Tunnelauskleidungen mit Tübbingen und deren verfahrenstechnische Voraussetzungen. DGGT Baugrundtagung Hannover 2000.
Zaheri, M., Ranjbarnia, M., 2021. Ground reaction curve of a circular tunnel considering the effects of the altered zone and the self-weight of the plastic zones. Eur. J. Environ. Civ. Eng. 26 (11), 4973–4997. https://doi.org/10.1080/19648189.2021.1877829.
Zaheri, M., Ranjbarnia, M., 2022. Long-Term Analysis of Tunnels in Rheological Rock Masses Considering the Excavation-Damaged Zone. Int. J. Geomech. 23 (1). https://doi.org/10.1061/(ASCE)GM.1943-5622.0002642.
Zaheri, M., Ranjbarnia, M., Dias, D., Oreste, P., 2020. Performance of segmental and shotcrete linings in shallow tunnels crossing a transverse strike-slip faulting. Transport. Geotech. 23. https://doi.org/10.1016/j.trgeo.2020.100333.
Zaheri, M., Ranjbarnia, M., Goudarzy, M., 2022. Analytical and Numerical Simulations to Predict the Long-Term Behavior of Lined Tunnels Considering Excavation-Induced Damaged Zone. Rock Mech. Rock Eng. 55, 5879–5904. https://doi.org/10.1007/s00603-022-02962-0.